# CMS Draft Analysis Note

*The content of this note is intended for CMS internal use and distribution only*

2014/09/23
Head Id: 168171
Archive Id: 163790:168171MP
Archive Date: 2013/01/29
Archive Tag: trunk

# Search for long-lived neutral particles decaying to photons

Shih-Chuan Kao, Yuichi Kubota, Tambe Norbert, and Roger Rusack
University of Minnesota



## Abstract

A search for long-lived neutral particle decaying into photons is performed using 19.1 $\text{fb}^{-1}$ of proton-proton collision data at $\sqrt{(s)} = 8\,\text{TeV}$. We present a method which exploring its long-lived feature by using the time measurement from the ECAL. A data-driven method to predict anonymous sources of background is also developed. The method is sensitive to the lifetime ($c\tau$) beyond 1000 mm. Taking GMSB as target model and applying our method to data, no significant excess is observed. An upper limit at 95% C.L. is set.

# 1 Introduction

After the observation of the new neutral boson at the LHC, it indicates strong possibility for the existence of the Standard Model Higgs and encourages the search for the physics beyond the Standard Model. Since many theories suggest the format of long-lived particles, most possible candidate is neutralino ($\tilde{\chi_0}$) which decays into a photon and a weakly interacting stable gravitino ( $\tilde{G}$) that is invisible for the CMS detector. Therefore, the photons and missing energy from event topology are the signature.

Base on CMS detector, the fine granularity and great energy and timing resolution of CMS electromagnetic calorimeter (ECAL) becomes the useful applications to search long-lived neutral particles decaying to photons.

In current scheme of the Standard Model, there is no direct physics process from TeV level proton-proton collisions showing the delayed timing. Therefore, the use of ECAL timing provides a great application to perform the search with nearly zero background. In this study, we explore the features of topological parameters of cluster shape and timing from ECAL and applied them to the search of long-lived neutral particle decaying to photons.

# 2 Data and Monte Carlo samples

The data used in the analysis was collected during 2012 runs with integrated luminosity of 19.1 $\text{fb}^{-1}$. The dataset is summarized in table 1. The Monte Carlo (MC) samples are generated by `PYTHIA 6` with an extenal SLHA (Supersymmetry Les Houches Accord) file. SLHA file was The generation for signal samples adopt SUSY GMSB(Gauge-Mediated Supersymmetry Breaking) scheme where the free parameters, the SUSY breaking scale ($\Lambda$), and the $\tilde{\chi_0}$ lifetime ($c\tau$) are varied to cover an appropriate range of phase space. In this analysis, the $\Lambda$ is fixed at 180 TeV and the $c\tau$ is varied from 250 mm to 6000 mm. For the background, there is no specific process which causes the real time delay from the collisions. Therefore, $\gamma+$ jets samples are just used for timing calibration and sanity check. The samples from Monte Carlo simulation are listed in table 2 and table 3.

| Dataset Name | Recorded Luminosity [ $\text{fb}^{-1}$ ] |
|---|---|
| `Run2012B-EXODisplacedPhoton-22Jan2013-v1` | 5.1 |
| `Run2012C-EXODisplacedPhoton-19Dec2012-v1` | 6.9 |
| `Run2012D-EXODisplacedPhoton-19Dec2012-v1` | 7.1 |
| `/Run2012C/Cosmics/Run2012C-22Jan2013-v1/RECO` | 3130384 (events) |
| `/Run2012D/Cosmics/Run2012D-22Jan2013-v1/RECO` | 52430 (events) |

Table 1: The dataset name and corresponding integrated luminosity of the data used in the analysis

| $c\tau$ ( mm) | $\sigma_{LO}$ (pb) | number of events |
|---|---|---|
| 250 | 0.0145 | 50112 |
| 500 | 0.0145 | 50112 |
| 1000 | 0.0145 | 50112 |
| 2000 | 0.0145 | 50112 |
| 3000 | 0.0145 | 50112 |
| 4000 | 0.0145 | 46944 |
| 6000 | 0.0145 | 50112 |

Table 2: The signal GMSB MC samples used in this analysis

| $\hat{p_T}$ | $\sigma_{LO}$ (pb) | number of events |
|---|---|---|
| $50 \sim 80$ | 3322.3 | 1995062 |
| $80 \sim 120$ | 558.3 | 1992627 |
| $120 \sim 170$ | 108.0 | 2000043 |
| $170 \sim 300$ | 30.1 | 2000069 |
| $300 \sim 470$ | 2.1 | 2000130 |
| $470 \sim 800$ | 0.212 | 1975231 |

Table 3: The $\gamma+$ jets samples used in this analysis

# 3 ECAL Time

The ECAL Time is the main observable from the signal in this study. The time measurement is from the readout of the Avalanche Photo-Diode (APD) of ECAL which is determined from the raising edge of the pulse shape. Since an ECAL cluster of a photon object contains many crystals, we examed two different timing information in order to find out the most accurate way to retrieve timing information of the photon and reject the background, which are listed below.

- Seed time: ECAL Time form the seed crystal of the seed basic cluster of photon object.
- Cluster time: The weighted averaged time from all crystals in the seed basic cluster (equation 1). A normalized $\chi^2$ cut ($\chi^2 < 4$) is imposed.

$$T_{cluster} = \frac{\sum_i t_i \times \frac{1}{\sigma_i^2}}{\sum_i \frac{1}{\sigma_i^2}} \tag{1}$$

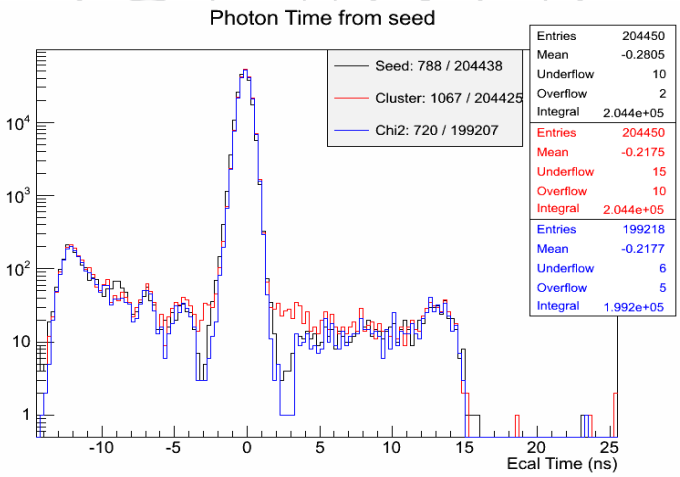


Figure 1: The timing distribution for inclusive single photon events

According to their performance, seed time and cluster time both have similar value and resolution. We choose seed time of photon because seed time could possibly reveal the nature of different background sources such as halo or spikes in which pileup could potentially contribute to their cluster.

However, the cluster time still can be used to address the time of a jet since its electromagnetic components usually doesn't belong to a single particle. Therefore, jet time is used as a cross-

check for event time if it is available. As shown in figure 2, jet time and photon time are correlated and all jet time are within 3 ns window.

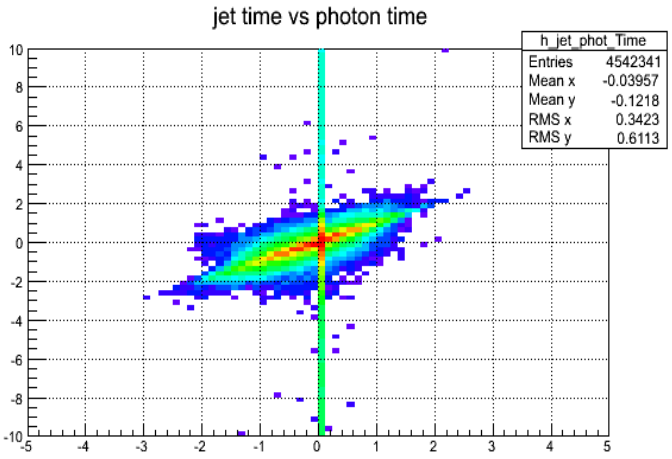


Figure 2: The jet and photon time correlation

The long lifetime of neutralino is the main reason of the delay timing which results in the photon decayed away from primary vertex. It implies that the delay is either from the slow motion of neutralino or the angular deviation of decay photon with respect to the neutralino. Two quantities, $\Delta t1$ and $\Delta t2$, are defined to examine the contribution from both effects (figure 3) :

- $\Delta t1$ = (L1/c$\beta$) - (L1/c)
- $\Delta t2$ = (L1 + L2 - L3)/c

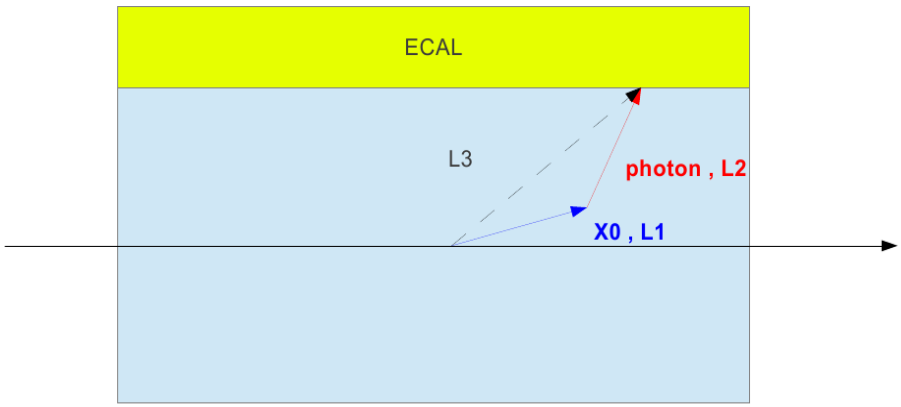


Figure 3

Comparing with ECAL time, (L1/c$\beta$) + L2/c - (L3/c), $\Delta t1$ measures the delay from the neutralino's motion and $\Delta t2$ gives the delay from the deviation of the photon path assuming neutralino is at the speed of light. The distribution of $\Delta t1$ and $\Delta t2$ from signal MC sample (shown in figure 4) for delay photon events indicates that the slow motion of neutralino is the main cause for the delay ECAL time. Moreover, the decayed photon from neutralino is tend to move in the same direction of neutralino due to the boost of neutralino.

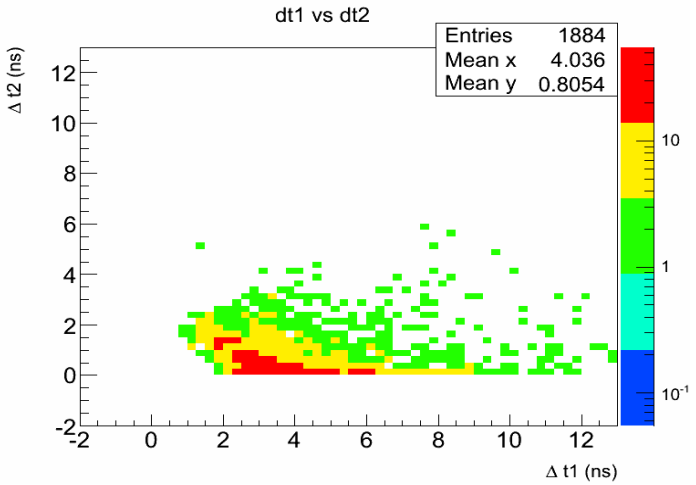


Figure 4: $\Delta t1$ and $\Delta t2$ distribution of GMSB sample ($\Lambda$ 180 TeV and $c\tau$ 6000 mm)

The time resolution is measured by fitting the time distribution from $\gamma+$ jets samples. The MC samples are generated in a wide $\hat{p_T}$ range from 50 GeV to 800 GeV. A control sample from data is selected by requiring one isolated photon, one or two jets and $\not{E}_T$ less than 30 GeV in events. Comparing results from MC and data, it suggests that the central value of timing from MC need to be shifted about 125 ps and an additional smearing on resolution is also required (Figure 5).

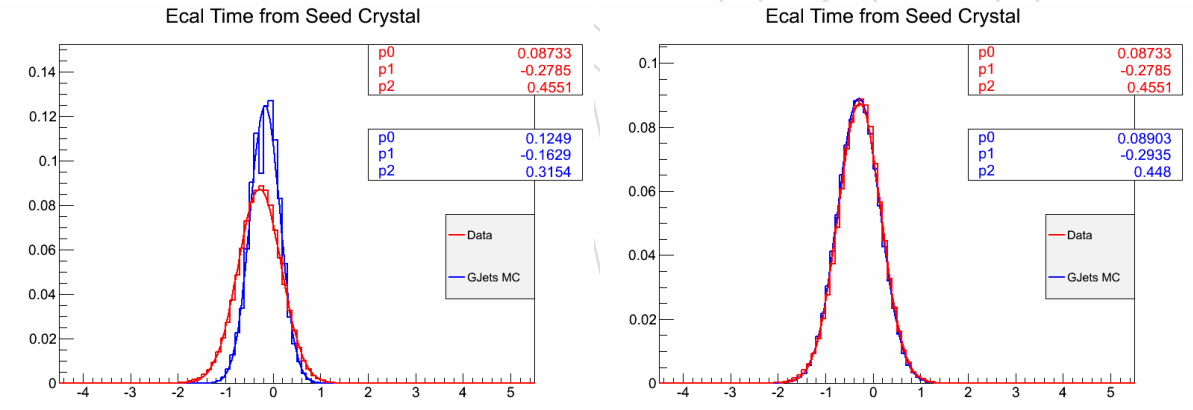


Figure 5: The comparison between time distribution between $\gamma+$ jets MC (blue) and Data (red) before (left) and after (right) calibration

# 4 Event and Object Selection

Since photons decayed from long-lived neutral particle is the main signature from the signal, it not only implies that the distinguishable timing difference between signal and background but also suggests that the photon does not necessarily points to the CMS interaction point. The crystals of the CMS ECAL detector are pointing to the mean position of the primary interaction vertex which implies a round shape of ECAL cluster for photon objects from collision.

Therefore, the ECAL cluster shape also can be used to distinguish signal and background since the photon decayed from long-lived neutralino can be away from primary vertex. An earlier study already demostrate the selection of off-pointing photon by using variable $S_{major}$ and

$S_{minor}$ [1, 2], where $S_{major}$ is the major axis and $S_{minor}$ is minor axis of the elliptical shape of ECAL cluster. Based on the study in section 3, one major source of late photon is from slow motion of neutralino. In this scenario, the deviated angle from neutralino's momentum is not necessary large. A certain constraint on $S_{major}$ or $S_{minor}$ for signal selection would lower the signal efficiency. Thus, a range of $S_{major}$ and $S_{minor}$ (section 5.3) is only set to exclude anomalous ECAL spikes.

Another common feature for long-lived neutral particles events is missing energy. Since gravitino ( $\tilde{G}$) is undetectable for the CMS detector, significant amount of missing energy is expected in event topology. A cut on $\not{E}_{\mathrm{T}}$ is also useful to lower the rate from the standard model backgrounds like $\gamma+$ jets process and QCD events (Figure 6).

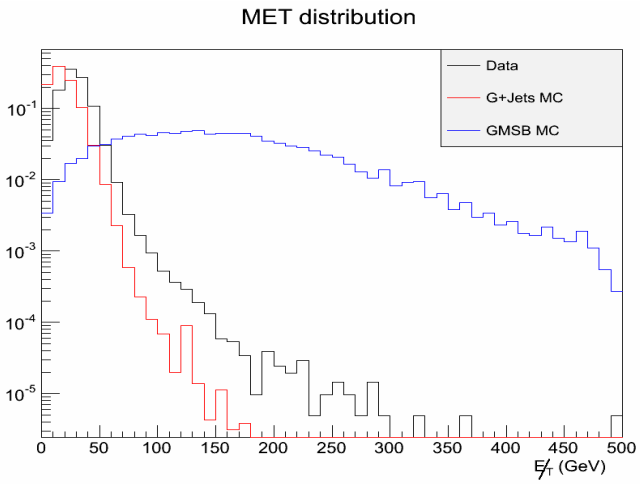


Figure 6: The $\not{E}_{\mathrm{T}}$ distribution for data and MC samples

## 4.1 Trigger

The events are selected online using the trigger, HLT_DisplacedPhoton65_CaloIdVL_IsoL_PFMET25. The trigger was developed to devote displaced photon analysis. In order to decrease model dependency, the trigger only require one isolated photon with $p_{\mathrm{T}}$ threshold 65 GeV and particle flow $\not{E}_{\mathrm{T}}$ above 25 GeV. Due to large rate of ECAL spikes, a range of $S_{minor}$ ($0.1 < S_{minor} < 0.4$) is set in HLT processes to lower the rate (Figure 7).

The efficiency and turn-on curve are studied separately for two objects, photon and $\not{E}_{\mathrm{T}}$, in trigger definition. In order to decouple correlation between photon and $E_{\mathrm{T}}^{\mathrm{miss}}$, single muon dataset (HLT_IsoMu30) is used for efficiency measurement. The photon in the event must pass offline selection (see next section) and its ECAL time must be within 2 ns ($|t| < 2$ ns). The photon efficiency is measured under the presence of HLT PFMET object with $p_{\mathrm{T}}$ greater than 25 GeV. Similar to photon, the efficiency of missing $E_{\mathrm{T}}$ is measured if there is a HLT photon object with greater than 65 GeV $p_{\mathrm{T}}$ in the event. The result is shown in Figure 8.

## 4.2 Offline Event Selection

In order to have less model dependence, the offline selection imposed less dependence on jet multiplicity which relates to the final state of the event topology and required at least one photon in the event. Due to large rate of ECAL spikes and its nature of negative timing, the normal photon reconstruction constrained the use of ECAL crystals with ECAL time in a 3 ns window ($|t_{crystal}| < 3$ns). This results in a cut-off at 3 ns for normal photon object. Therefore,

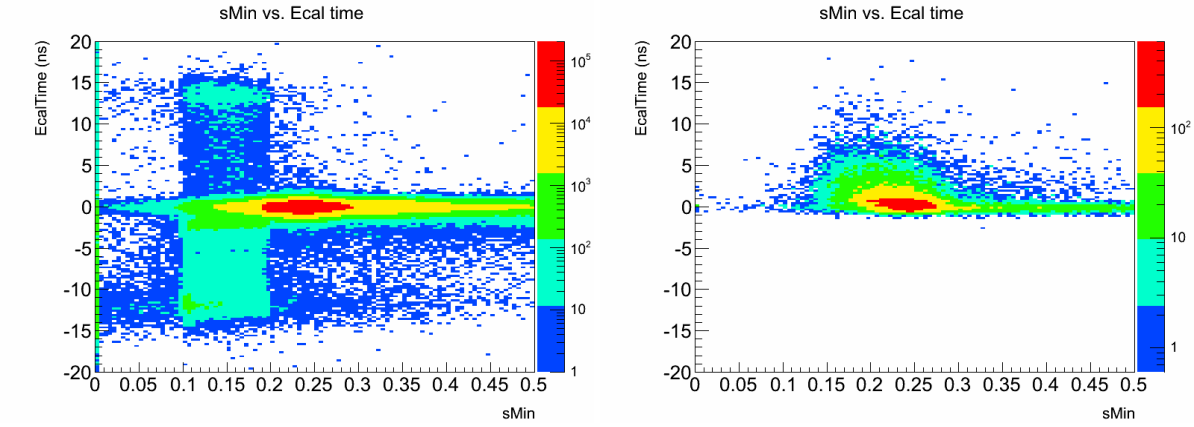


Figure 7: The $S_{minor}$ v.s. ECAL time distribution for Data (left) and GMSB MC (right). The data sample has been pre-selected by HLT trigger

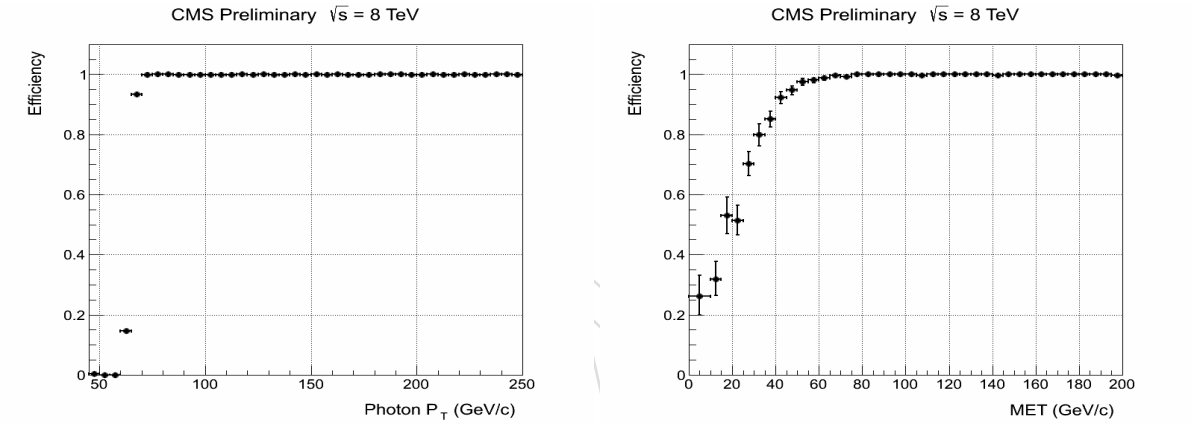


Figure 8: The trigger efficiency turn-on curve for the photon $pT$ with $\not{E}_{\mathrm{T}} > 25$ GeV (left) and for $\not{E}_{\mathrm{T}}$ with photon $p_{\mathrm{T}} > 80$ (right)

the photon reconstruction was re-processed with the setup which is extended to include those "out-of-time" crystals. However, this recovery does have the disadvantage to bring back those out-of-time machine induced background such as halo or spikes. (Figure 9). The summary for photon selection are listed below:

- The $p_{\mathrm{T}}$ of leading photon is greater than 80 GeV. Other photons in the event must have $p_{\mathrm{T}}$ greater than 45 GeV
- Photon from ECAL Barrel, i.e. $|\eta| < 1.47$
- H/E $< 0.05$
- $\Delta R(track, photon) > 0.6$
- $0.12 \leq S_{minor} \leq 0.38$

For jets and $\not{E}_{\mathrm{T}}$ reconstruction, particle-flow algorithm is used which take tracking information into account for incomplete calorimeter measurement. However, particle-flow algorithm do not consider energy deposit from ECAL barrel if its ECAL time is outside the 3 ns window ($|t| > 3$ ns) as well as those from ECAL endcap with ECAL time greate than 10 ns ($|t| > 10$ ns). In this analysis, we compensated the constributions from these out-of-time photons in $\not{E}_{\mathrm{T}}$ calculation and redefined it as MET2. In the offline event selection, is not required to keep

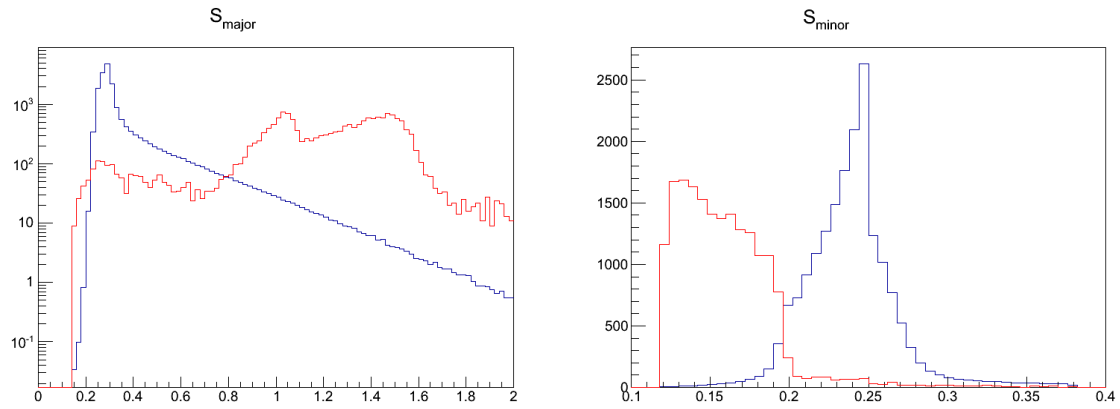


(a) (b)

Figure 9: The comparison between nominal photon sample (blue) and off-timing photon sample (red) for $S_{Major}$ and $S_{Minor}$

event but will be used in the background estimation after certain alternations. The jet selection criteria are listed below. Zero and one-jet events are considered as signal free and used for closure test of background estimation.

- Jet $p_{\mathrm{T}} > 35$ GeV.
- Number of constituents $> 1$
- Charged EM energy fraction (CEF) $< 0.99$
- Neutral hadronic energy fraction (NHF) $< 0.99$
- Neutral EM energy fraction (NEF) $< 0.99$
- If $|\eta|$ of the jet $< 2.4$, charged hadronic energy fraction (CHF) $> 0$
- If $|\eta|$ of the jet $< 2.4$, charged multiplicity (NCH) $> 0$
- $\Delta R$ (jet, photon) $> 0{,}3$

### 4.3 Efficiency and Acceptance

Under the constraint of the CMS ECAL geometry, the decay length of neutralino in the CMS lab frame affects the efficiency and acceptance for reconstruction and event selection. The decay length in lab frame is determined by neutralino's life time and its speed measured in lab frame. The efficiency of reconstruction and event selection shows that no dependence between different $c\tau$ models (figure 10a). A clear drop at 1500 mm reflect the outter surface of ECAL detector. The time acceptance is defined as the fraction of the photons with ECAL time greater than 3 ns. Thus the higher $c\tau$ value leads to higher acceptance (figure 10b). As discussed in section 3, there are two sources of delay photons from neutralino's decay. Each one has a different acceptance with respect to decay length. (figure 11)

## 5 Background Estimation

Since there is no known reaction from collisions has delayed photon production, the possible sources of background for late photon may come from bad timing measurement or fake photon objects which are not from collisions.

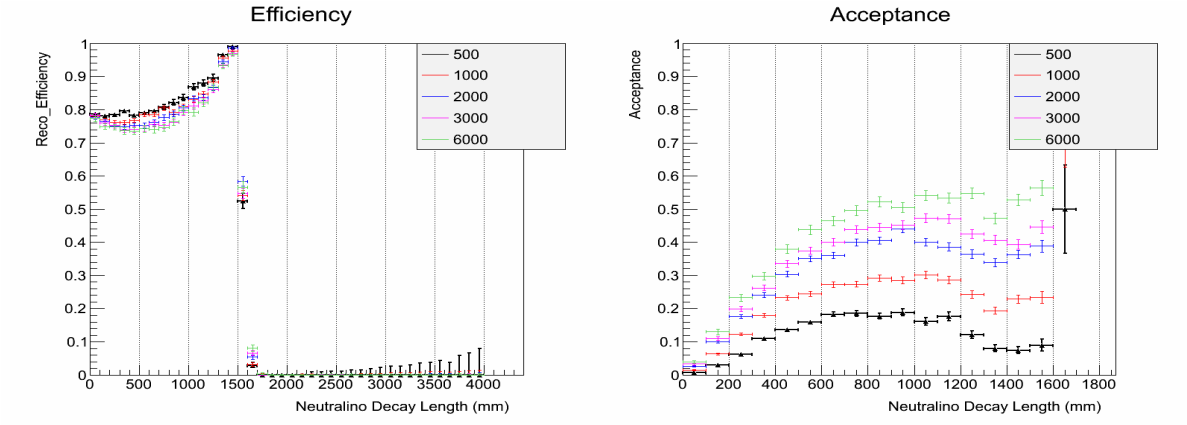


(a) (b)

Figure 10: The efficiency of reconstruction and selection and time acceptance with respect to transverse decay length in lab frame for different $c\tau$ values.

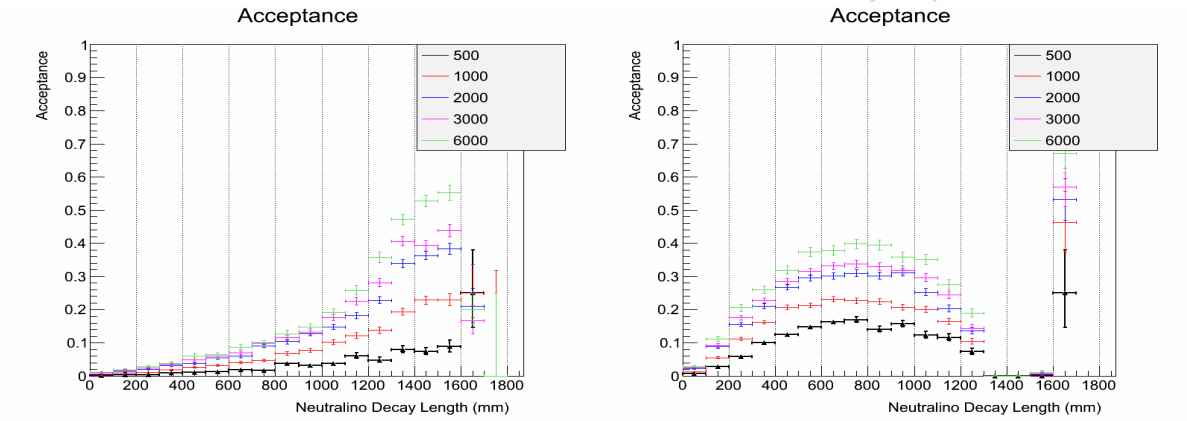


(a) (b)

Figure 11: The time acceptance with respect to transverse decay length in lab frame for late photons from slow neutralino (11a) and large decay angular (11b)

As mentioned in previous section, ECAL time is determined by the pulse shape. Since the time from seed scrystal is adopted, the seed of photon object becomes the issue of mis-measurement of timing and indication of its source.

In order to study the background behavior, an in-time photon sample and an off-time photon sample are defined. The nominal photons have ECAL time between -1 ns and 1 ns and are from the events contain at least two jets. The off-time photons are photons with ECAL time greater than 2 ns or smaller than -3 ns with no jet in the event. By comparing with these two samples, a summary of differences is listed belowed. Based on these phenomena, we classified background into three difference types, halo, anomalous ECAL spikes and cosmic-rays which are described in the following sections.

1. Clear matching between a CSC segment and their ECAL Cluster in off-timing sample (Figure 12).

2. Different $S_{Major}$ and $S_{Minor}$ population. Figure 13 shows the differences between in-time and off-time photons. The $S_{Major}$ with respect to $\eta$ and $\phi$ distribution (Figure 14) suggests possible more than one source of background.

3. Matching between a DT cosmic-ray segment and a photon cluster (Figure 15).

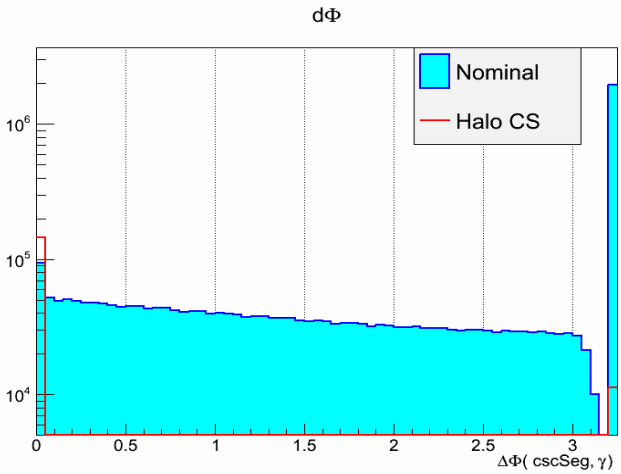


Figure 12: CSC $\Delta\phi$ distributions of in-time (blue) and off-time (red) samples.

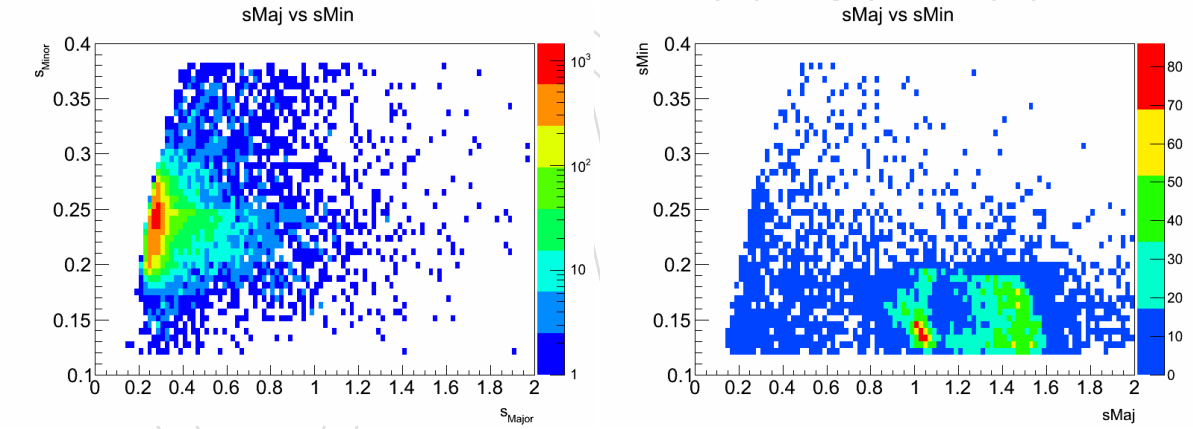


Figure 13: The comparison between nominal photon sample (left) and off-timing photon sample (right) for $S_{Major}$ and $S_{Minor}$

Based on their features, the parameters used to identify them are listed below after studies using corresponding control samples.

- CSC$\Delta\phi$, the $\phi$ difference between a CSC segment and a photon cluster.
- $S_{Major}$ and $S_{Minor}$.
- DT$\Delta\phi$ and DT$\Delta\eta$, the $\phi$ and $\eta$ difference between a DT cosmic-ray segment and a photon cluster.

## 5.1 Halo Photon

Beam halo muons are known existing particles created by collsions of beam gas or scratching collimator from beams while some of them hit and bremsstrahlung in the CMS ECAL detector

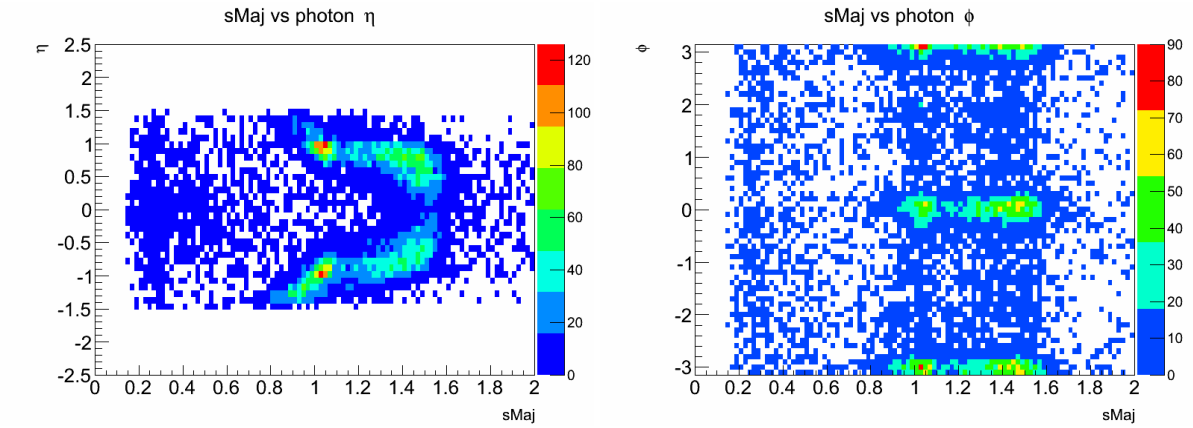


Figure 14: $S_{Major}$ distributions of off-timing sample

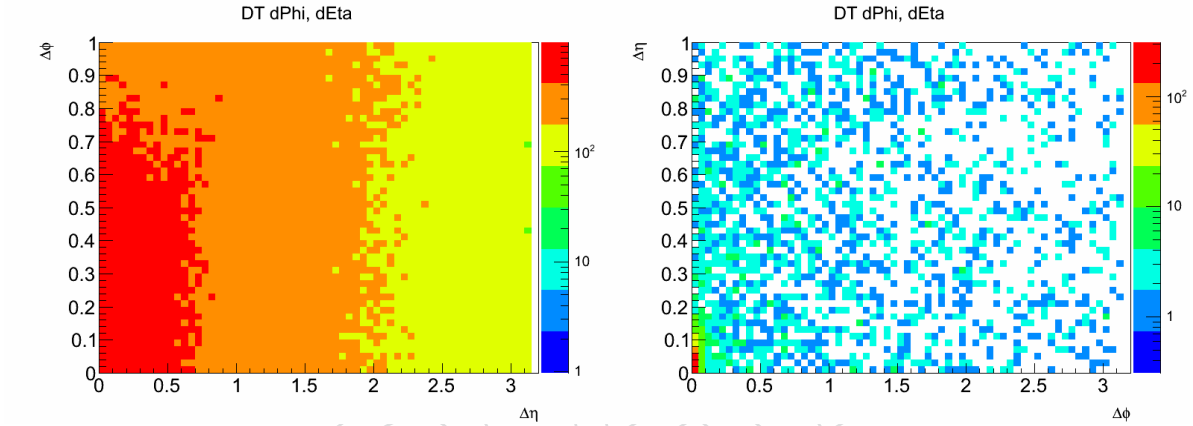


(a) In-time (b) Off-time

Figure 15: DT $\Delta\eta - \Delta\phi$ distributions of in-time (left) and off-time (right) photon samples.

which create photon like objects. Since they are created by halo muons, a possible muon track can be found in the Endcap muon system. Our study shows that a clear matching between a CSC segment and ECAL cluster is found (Figure 12). Additionly, the flying path of halo muons are nearly parallel to the beam which result in a different, long ellipse shower shape which is corresponding to a larger $S_{Major}$ and smaller $S_{Minor}$.

A simple approximation for the ECAL time from halo photons can be derived from

$$t_0 = \frac{r}{c} = \frac{\rho}{sin\theta}\frac{1}{c} \tag{2}$$

$$t_{halo} = \frac{z}{c} = \frac{\rho}{tan\theta}\frac{1}{c} \tag{3}$$

$$t_{ECAL} = t_{halo} - t_0 \tag{4}$$

$$= \frac{\rho}{c}\left(\frac{1}{tan\theta} - \frac{1}{sin\theta}\right) \tag{5}$$

$$= -\frac{\rho}{2c}tan(\theta/2) = -\frac{\rho}{2c}\exp^{-\eta} \tag{6}$$

where $\rho$ is the transverse radius with respect to beam pipe, $r$ is the distance between vertex and photon cluster, z is the z position of the photon cluster, c is the speed of light, $\theta$ is azimuthal angle. The reference time ($t_0$) is the function of $\eta$. This equation is under the assumption that halo muons travel parallel to the beam. The ECAL time for halo photons is the time with respect to $t_0$, the time assumed that the ECAL cluster is orignated from primary vertex. Therefore, the ECAL time of halo photons is a function of $\eta$ and ealier than the time of photons from the associated collisions.

Due to 400 MHz RF frequency of the LHC, it provides 9 more LHC buckets for proton fills. The satellite bunches are thus formed by the causes of beam captured in incorrect locations at each stage of beam transfer between different stages. The existence of satellite bunch halo can be observed from the Endcap ECAL system and identified by selecting the photon cluster matched with a CSC segment. A clear patten in 2.5 ns can be seen (Figure 16). Consequently, the halo from later arrival satellite bunches could bring late photons.

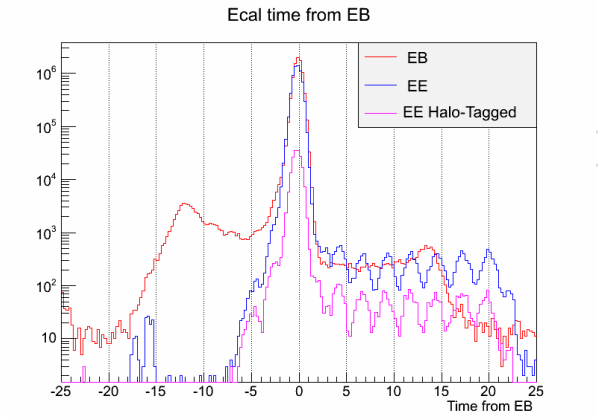


Figure 16: The ECAL time of photons from EB and EE. The periodic pattern is from the halo of satellite bunches.

Based on this estimation, a halo sample can be extracted by using this equation (Figure 17).

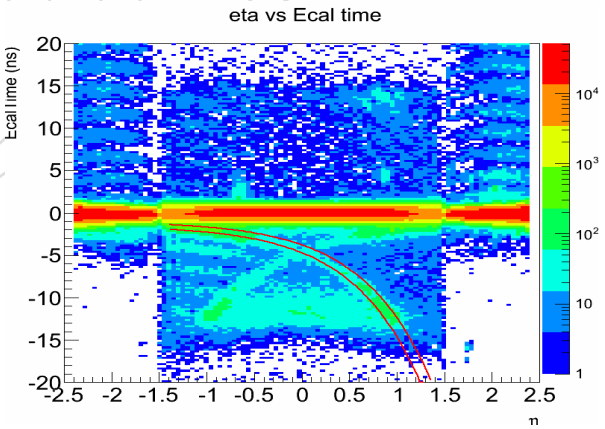


Figure 17: The $\eta$ v.s. ECAL time for photons. The red curves show the fitting range to select halo control sample.

By cross examing various variables, a halo control sample can be refined by adding following criteria:

- The $\phi$ of the candidate must be around 0 or $\pi$ ($|\phi - 0| < 0.2$ or $|\phi - \pi| < 0.2$).
- ECAL time of the halo candidate must be less than -3 ns.
- 0-jet events.

Using this control sample, we verify that the matching between a CSC segment and an ECAL cluster is the main character of halo photon. Additionaly, it also shows the long ellipse shape of ECAL cluster, large $S_{Major}$ and small $S_{Minor}$, because the shower was developed along the flight path of the halo muon, which is across crystals. Therefore, two rules to identify halo photon were concluded as

- $\Delta\phi$ between a CSC segment and a photon cluster must be smaller than 0.05.
- $0.8 < S_{Major} < 1.65$ and $S_{Minor} < 0.2$.

and its efficiency can be determined by using this control sample. Mis-tagging rate can be obtained from nominal sample (Figure 18). The mis-tagging rates for both sources are measured using the $\gamma+$ jets like events (at least two jet and $\not{E}_{\mathrm{T}} < 60$ GeV) with ECAL time $|t| < 1$ ns. According to the halo control sample, $S_{major}$ shows the dependency with $\eta$. Thus the efficiency and mis-tagging rates for halo component are evaluated in 5 different $|\eta|$ slices from 0 to 1.47.

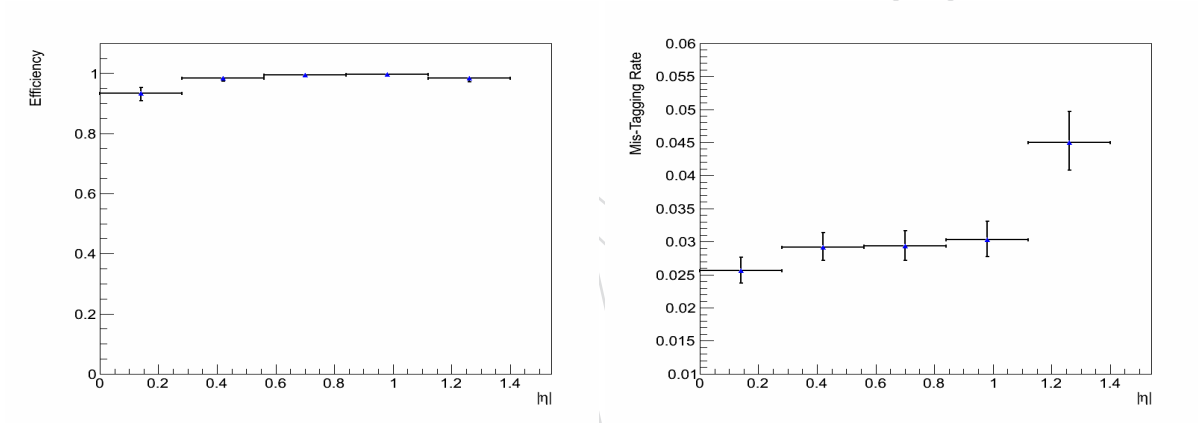


Figure 18: Tagging efficiency and mis-tagging rate for halo photons in 5 $\eta$ regions

## 5.2 Cosmic-Ray

Similar to halo photons, cosmic-rays can possibily initiate showers in the ECAL. Their existence can be found by looking at the $\Delta\phi$ and $\Delta\eta$ between a DT cosmic-ray muon segment and an ECAL cluster. Due to the space between Muon Barrel system and ECAL, the actual DT positon used is projecting the position of DT segment to ECAL surface from its direction. A clear match at small $\Delta\phi$ and $\Delta\eta$ can be found from off-time photon sample (Figure 15b) in contract to in-time sample (Figure 15a).

A support study for this matching method using cosmic dataset is also performed (Figure 19). Since the contain of cosmic dataset is different from collision data, event selectin criteria for cosmic data use ECAL supercluster instead of reconstructed photon object and the seed crystal energy of the supercluster must be greater than 10 GeV. A 75.5% of the cosmic tagging rate is obtained while at least one DT segment and one ECAL supercluster are both presented in the the events. A 1.4% of fake rate for this method is obtained by using the good photon control sample from diplaced photon dataset where the events pass the regular event selection and the ECAL time must be within 1 ns window ($|t| < 1$ ns).

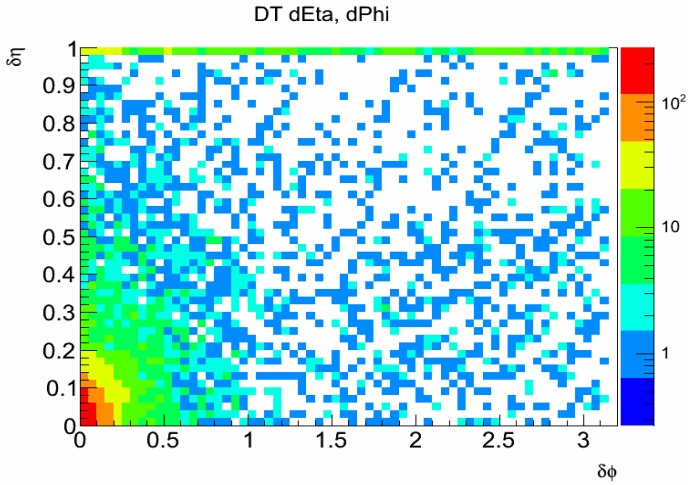


Figure 19: The $\Delta\eta$ and $\Delta\phi$ distribution of DT segment and ECAL supercluster for cosmic-ray data.

## 5.3 Anomalous ECAL Spike

ECAL spikes is known to be the energy deposit to the Avalanche Photo-Diode (APD) from direct ionization of charged particles from collisions [3]. Although the topological "swiss-cross" method is implemented in the reconstruction process to remove them, some of them are still observed due to its high rate. This component can be extracted from the negative timing sample where no correlation is found from other detectors such as muon endcap or muon barrel system for halo and cosmic-ray muons.

Due to its forming mechanism, its ECAL cluster size is expected to be smaller than the size of regular photons (Figure 20) and mostly has negative ECAL time because of its rapid rising edge of the signal pulse. Therefore, the second component in $S_{Major}$ distribution (Figure 14), the smaller $S_{Major}$ value and no $\eta$ or $\phi$ structure, can be addressed as the presence of ECAL spike. Based on their characters, the tagging criteria for spike candidate are defined below.

- Swiss-cross value $< 0.9$.
- $S_{Major} < 0.6$ and $S_{Minor} < 0.17$.

## 5.4 ABCD Method for Un-Tagged Background and QCD

The survived photon objects after applying three background tagging are estimated by using a ABCD method. The two parameters used in this ABCD method is ECAL time and missing transverse energy. In this analysis, the missing transverse energy from particle flow reconstruction is adopted. However, the particle flow algorithm take the photons into account if the photon object from EB has ECAL time within 3 ns window and the photon from EE has ECAL time within 10 ns window.

Therefore, two different missing transverse energy are defined in term of the contribution from photons. Regardless timing of the photon object, MET1 is the missing transverse energy without counting photon's contribution in the event. MET2 is the convention definition of missing transverse energy. Therefore, the off-timing photons ( $|t| > 3$ns in EB and $|t| > 10$ ns in EE) should added in the calculation. In other words, MET2 is the vector sum of MET1 and photon's $p_T$.

According to MET1 and MET2, the non-collision backgrounds such as halo, spikes and cosmic-

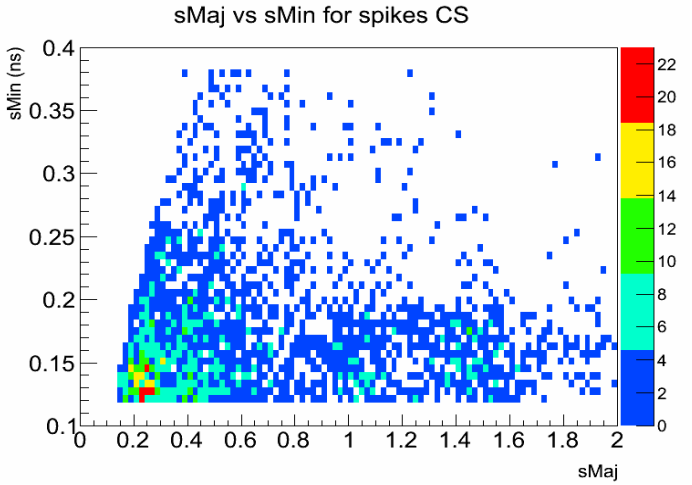


Figure 20: $S_{Major}$ and $S_{Minor}$ distribution of spike control sample.

ray would have higher MET2 but small MET1 since the photon objects do not belong to the events. On the other hand, the collision backgrounds spread in MET2, small MET2 refer to QCD type of events, events with large MET2 could be from W, Z or top quark productions. However, collision events would mostly have large MET1 since the event topology most has at least one photon and the photons are not account for MET1 calculation. (Figure 21)

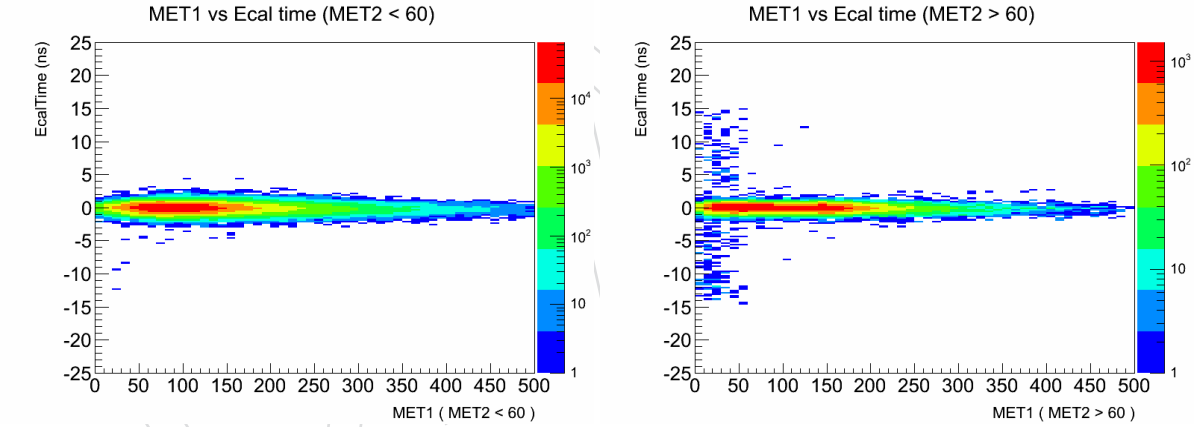


Figure 21: MET1 v.s. ECAL Time distributions for MET2 $<$ 60 GeV (left) and MET2 $>$ 60 GeV (right) events.

The ABCD regions are defined from ECAL time and MET1 which is shown in table 4. A and B regions are signal free region since their $|t| < 3$ ns. Region C is also signal free and non-collision enhanced because events contain photon from collision should mostly have large MET1. Thus, the non-collision background in signal region D can be estimated from

$$\text{Un-tagged background in D} = \frac{B}{A} \times C \tag{7}$$

As for possible contemination from collision events, an another ABCD method using ECAL time and MET2 is developed. Since ECAL time from collision type events should be around zero, the $|t| <$ 2ns region can be acted as control region for extracting background behavior. The definition of this QCD estimation ABCD is shown in table 5 and the collision background

in D region can be estimated by

$$\text{Collision background in D} = \frac{F}{F'} \times D' \tag{8}$$

Similar to the collision background in D, the same formula also applicable to A,B and C regions. By substracting the QCD contributions in A,B and C regions, it provides purer un-tagged background estimation. Combinition all the estimation. The final background can be determined by

$$\text{Total background in D} = (\frac{B - Q_b}{A} \times C) + Q_d \tag{9}$$

$$Q_d = \frac{F}{F'} \times D' \tag{10}$$

$$Q_b = \frac{F}{F'} \times B' \tag{11}$$

| MET2 $>$ 60 GeV | MET1 $<$ 60 GeV | MET1 $>$ 60 GeV |
|---|---|---|
| $t >$ 3 ns | C | D |
| $\|t\| <$ 2 ns | E | F |
| $t <$ -3 ns | A | B |

Table 4: ABCD definition for un-tagged non-collision backgrounds

| MET1 $>$ 60 GeV | MET2 $<$ 60 GeV | MET2 $>$ 60 GeV |
|---|---|---|
| $t >$ 3 ns | D′ | D |
| $\|t\| <$ 2 ns | F′ | F |

Table 5: ABCD definition for collision background

A closure test is done by using 0 and 1-jet events. The results can be found at table 6 and table 7. After applying the numbers, the estimated background in D region for 0 and 1-jet events is 6.44 ($^{+2.947}_{-3.448}$) which is compitable with observed value 5. The uncertainty from collision background has trivial effect because the ratio F/F′ is small.

$$\text{D} = (\frac{6 - 0.13}{88} \times 95) + (0.1) = 6.44^{+2.947}_{-3.448} \tag{12}$$

$$Q_d = \frac{34543}{1353685} \times 4 = 0.10 \pm 0.86 \tag{13}$$

$$Q_b = \frac{34543}{1353685} \times 5 = 0.13 \pm 1.07 \tag{14}$$

## 5.5 Cross-Check From Z Events

A cross-check for collision events is done using $Z \rightarrow e^+e^-$ events. This study use Z mass spectrum to extract Z and the background sample. Since Z decays promptly, the timing from the electrons must be in-time. The majority of the background is Drell-Yan process, which also have in-time electrons in the final state. However, any off-time electron could also pass event selection and present in the Z mass spectrum as well (Figure 22). Therefore, the time

| MET2 $>$ 60 GeV | Spikes | Halo | Cosmic | Un-tagged | Sum |
|---|---|---|---|---|---|
| D | 0 | 22 | 23 | 5 | 50 |
| C | 3 | 1213 | 259 | 95 | 1570 |
| B | 0 | 313 | 18 | 6 | 337 |
| A | 62 | 5890 | 224 | 88 | 6264 |
| F | - | - | - | - | 34543 |

Table 6: Closure test for 0 and 1-jet events

| MET2 $<$ 60 GeV | Spikes | Halo | Cosmic | Un-tagged | Sum |
|---|---|---|---|---|---|
| D′ | 0 | 0 | 0 | 4 | 4 |
| C′ | 0 | 0 | 2 | 0 | 2 |
| B′ | 0 | 1 | 2 | 5 | 8 |
| A′ | 7 | 11 | 0 | 6 | 24 |
| F′ | - | - | - | - | 1353685 |

Table 7: Closure test for 0 and 1-jet events

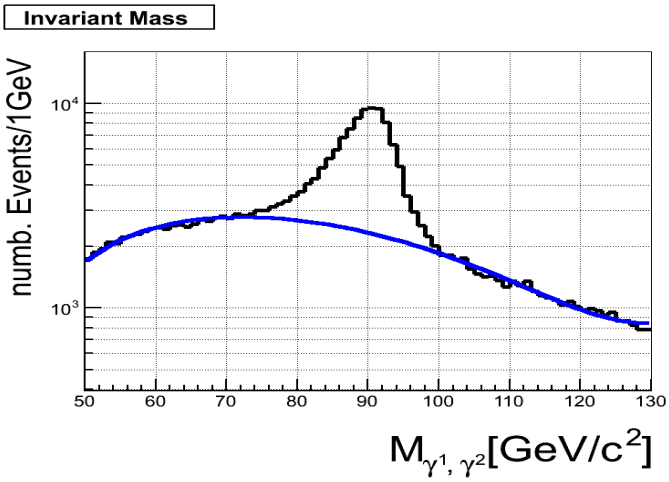


Figure 22: The invariant mass of two electrons

distribution from the off Z mass window sample provides a single background template with proper scale of two background sources. By substracting this background time distribution from the Z sample, a time distribution of pure Z events can be obtained.

The events requires at least two electrons with $p_{\mathrm{T}}$ greater than 30 GeV. The electron isolation is not applied due to the algorithm take off-time ECAL crystal into account of isolation deposit. The Z sample is chosen by requiring the invariant mass between 76 GeV and 100 GeV of leading two electrons (Figure 23a). For the background template, the sample is from the events with invariant mass between 50 to 76 GeV and 100 to 130 GeV (Figure 24a). By fitting the background shape in the mass spectrum, the background contamination in the Z sample can be estimated and the background template can be normalized properly.

Based on this pure Z time distribution, a ratio of $|t| < 2$ ns and $t > 3$ ns is 0.000046. This ratio can apply to the number from F region defined in previous section (34543) in order to verify the estimation of collision background in D region. This method estimates $1.58 \pm$ xx photons in D region which is consistent with the result ($0.1 \pm 0.86$) from the ABCD method.

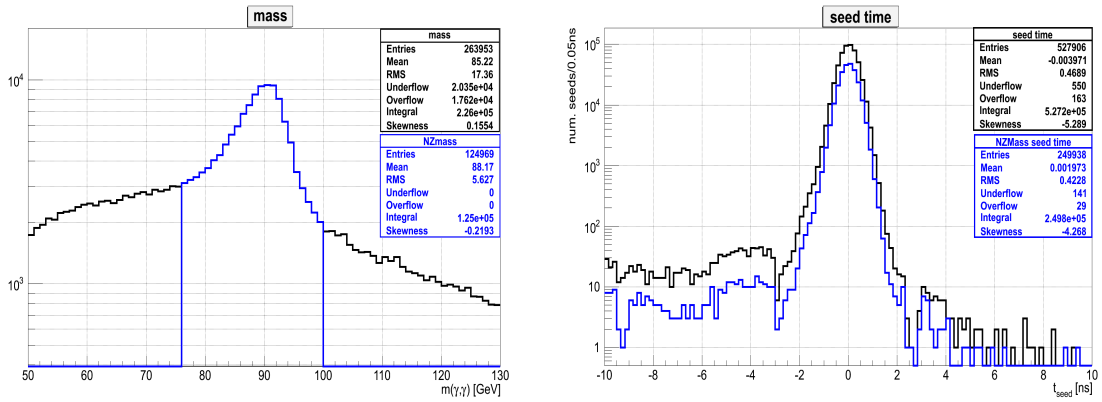


(a) (b)

Figure 23: The time distribution for Z candidate ( 76 GeV $<$ *Mass* $<$ 100 GeV) and background sample.

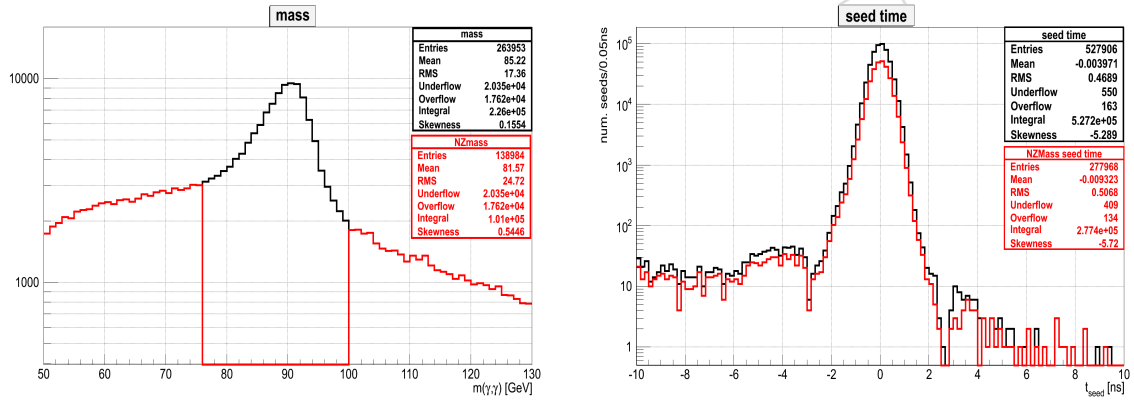


(a) (b)

Figure 24: The time distribution for Z candidate ( 76 GeV $<$ *Mass* $<$ 100 GeV) and background sample.

# 6 Systematic Uncertainties

The systematic uncertainties are taken into account of jet energy scale, jet energy resolution, $\not{E}_{\mathrm{T}}$, egamma energy scale as well as photon timing resolution.

# 7 Result

The upper limit at 95 % C.L. is set (Figure 25) by using CLs method. The result shows that ECAL timing method has sensitivity to long-lived neutralino from $c\tau$ 500 mm to 6000 mm.

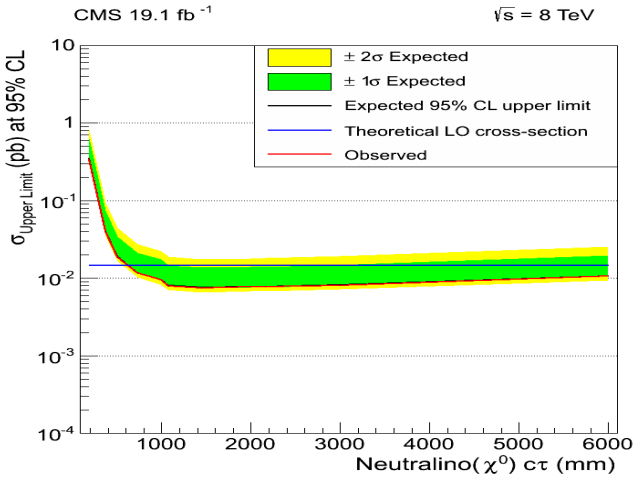


Figure 25: The upper limit at 95 % C.L. using $CL_s$ method

# 8 References

## References

[1] D. d. R. D. Franci, S. Rahatlou, "An algorithm for the determination of the flight path of long-lived particles decaying into photons", *AN-10-212* (2010).

[2] M. S. Daniele Del Re, Shahram Rahatlou and L. Soffi, "Search for Long-Lived Particles using Displaced Photons in pp Collisions at $\sqrt{s}$ = 7 TeV", *AN-11-081* (2012).

[3] CMS Collaboration, "Characterization and treatment of anomalous signals in the CMS Electromagnetic Calorimeter", *AN-10-357* (2011).